Available online at www.sciencedirect.com
SCIENCE DIRECT®
Journal of Sound and Vibration 291 (2006) 604–626
JOURNAL OF SOUND AND VIBRATION
www.elsevier.com/locate/jsvi

Alternate methods for characterizing spectral energy inputs based only on driving point mobilities or impedances

Seungbo Kim, Rajendra Singh*

Acoustics and Dynamics Laboratory, Department of Mechanical Engineering, The Center for Automotive Research, The Ohio State University, Suite 255, 650 Ackerman Road, Columbus, OH 43202, USA

Received 26 February 2004; received in revised form 15 June 2005; accepted 21 June 2005
Available online 2 September 2005

Abstract

This article analyses three characterization methods for spectral energy inputs to a linear time-invariant system. Analytical frequency domain formulations are examined for discrete vibratory systems and one-dimensional continuous structure (undergoing longitudinal or flexural motions) given a harmonic force excitation. Two existing methods that have been proposed by prior researchers are first critically examined. In particular, the driving point transfer functions and their derivatives with respect to frequency are analyzed for an appropriate application to the energy characterization scheme and to determine the sources of error. Then, a new (third) scheme is proposed that is more suitable over low and mid frequency regimes, based on a proper interpretation of the driving point mobilities or impedances and their derivatives. The new method is found to be insensitive to the driving point mobility or impedance formulations, unlike the existing methods. It does yield consistent results, without requiring a prior knowledge of the transfer functions. Finally, the role of structural loss factor has been clarified in the context of the stated problem.

1. Introduction

Vibratory state of complex structures is sometimes described in terms of limited degrees of freedom since the measurement at all internal and external points of a system, for instance, is rather difficult if not impossible. The utilization of the driving point frequency response functions

*Corresponding author. Tel.: +1 614 292 9044; fax: +1 614 292 3163.
E-mail address: singh.3@osu.edu (R. Singh).

0022-460X/$ - see front matter © 2005 Elsevier Ltd. All rights reserved.
doi:10.1016/j.jsv.2005.06.026

Nomenclature

A, B, C, D arbitrary constants
d damping matrix
E Young's modulus
E energy
f force amplitude
F force amplitude vector
I area moment of inertia
IL insertion loss
j $\sqrt{-1}$
k stiffness matrix
k stiffness
L length
m mass
m inertia matrix
M mobility
M mobility matrix
q moment amplitude
$\boldsymbol{Q}$ arbitrary constant
S area
v velocity
V velocity vector
Z impedance matrix
z impedance
α correction factor
Δ difference between zero-crossing frequencies
κ wavenumber
ϕ phase
ξ displacement
x, y, z cartesian coordinates
η loss factor
ρ mass density
ω frequency, rad/s

Subscripts

1, 2, 3, 4 characterization method
B flexural or bending motion
D driving point
d dissipated energy
i, j indices for elements
k potential energy
L axial or longitudinal motion
M energy estimation based on the mobility formulation
m kinetic energy
x, y, z cartesian coordinates
Z energy estimation based on the impedance formulation

Superscripts

T transpose
$\sim$ complex valued
* complex conjugate
$-$ time-averaged
$\hat{}$ estimate
$'$ real part
$''$ imaginary part

Operators

Re real part
Im imaginary part
Π permutation
$\partial/\partial\omega$ pseudo derivative with respect to frequency

alone is one extreme example of such approaches. Several vibratory energy (or power) analysis methods have described vibro-acoustic measures only at the driving points [1–6]. Both deterministic and statistical methods have been employed. Though these cover a broad range of frequencies, most methods have been applied primarily to the higher frequency regime [6]. Such methods [1–6] tend to focus on the dissipated power concepts although the determination of kinetic and potential energy spectra may be more appropriate to describe the dynamic interactions within the system, especially at the lower frequencies. Nevertheless, suitable methods that could truly characterize spectral kinetic and potential energy inputs to a vibratory system are, in general, not available. Recently, Pavic [7] examined the relationship between the global energy and

damping within the dynamic systems but the applicability of this relationship would strongly depend on the global damping values.

Our article attempts to develop a new spectral energy input characterization method with applicability over the low and mid frequency regimes. This would be based on the knowledge of driving point mobility or impedance. Earlier, Bobrovnitskii has proposed a method to characterize the vibrational energy inputs to structures [8]. This method (designated in our article as Method 1) attempted to identify the total time-averaged kinetic and potential energies within structures by using the driving point transfer functions, force and velocity but without the prior knowledge of the overall system matrix and/or the entire velocity field. However, the validity of the proposed formulation was limited to undamped structures as it produced erroneous predictions for damped structures. An alternate scheme (designated here as Method 2) was then presented by Bobrovnitskii and Korotkov [9]. It improves the energy prediction by numerically examining the error in energy estimates from Method 1. However, the use of Method 2 is still limited to a lightly damped structure at low and mid-frequencies [9]. An appropriate method is still not available for a heavily damped system and/or at higher frequencies that would correctly predict the total time-averaged energies based on the driving point information alone.

In this article, we critically assess and extend the prior analyses that are designated as Methods 1 and 2 [8,9] and analytically investigate the energy characterization issues in both discrete and continuous systems over low and mid frequency regimes. The scope is limited to a linear time-invariant system and the analysis is performed only in the frequency domain given a single harmonic force excitation. Specific objectives of our study include the following: (1) Examine the existing methods [8,9] that characterize the spectral energy input to a discrete system using only the driving point impedances or mobilities. (2) Analyze the driving point transfer function expressions and their derivatives with respect to frequency for proper interpretation to determine the sources of error. (3) Propose a new method (designated as Method 3 in this article) to estimate the spectral energies via the driving point transfer functions. (4) Develop the energy estimates for a clamped–free beam (in both longitudinal and flexural motions) and compare Methods 2 and 3, and clarify the role of structural damping.

2. Existing methods

2.1. Method 1

The method first proposed by Bobrovnitskii [8] is briefly summarized here. If the overall discrete system model including the sinusoidal velocity field and transfer functions are known, total time-averaged energy input (E) is identified by using the following equations where the ubiquitous harmonic term $e^{j\omega t}$ is omitted for the sake of brevity:

$$\tfrac{1}{2}\mathbf{V}^{*\mathrm{T}}[\mathbf{Z}/\omega]\mathbf{V} = \tfrac{1}{2}\mathbf{V}^{*\mathrm{T}}[(\mathbf{m} - \mathbf{k}/\omega^2)\mathrm{j} + \mathbf{d}/\omega^2]\mathbf{V} = [(\bar{E}_m - \bar{E}_k)\mathrm{j} + \bar{E}_d], \tag{1}$$

$$\tfrac{1}{2}\mathbf{V}^{*\mathrm{T}}[\partial\mathbf{Z}/\partial\omega]\mathbf{V} = \tfrac{1}{2}\mathbf{V}^{*\mathrm{T}}[(\mathbf{m} + \mathbf{k}/\omega^2)\mathrm{j} - \mathbf{d}/\omega^2]\mathbf{V} = [(\bar{E}_m + \bar{E}_k)\mathrm{j} - \bar{E}_d]. \tag{2}$$

Here, $\bar{E}_m$, $\bar{E}_k$ and $\bar{E}_d$ represent the time-averaged kinetic, potential and dissipation energies, respectively. Further, $\mathbf{Z}$, $\mathbf{m}$, $\mathbf{k}$ and $\mathbf{d}$ are the impedance, inertia, stiffness and damping matrices of

the complete system, respectively, and $\mathbf{V}$ is the velocity amplitude vector. Also, refer to the list of symbols for the identification. By taking sum and difference of Eqs. (1) and (2), the $\bar{E}_m$ and $\bar{E}_k$ terms are obtained as follows where Im represents the imaginary part of a complex quantity:

$$\bar{E}_m = \mathbf{V}^{*\mathrm{T}}\mathrm{Im}[\mathbf{Z}/\omega + \partial\mathbf{Z}/\partial\omega]\mathbf{V}/4, \tag{3}$$

$$\bar{E}_k = -\mathbf{V}^{*\mathrm{T}}\mathrm{Im}[\mathbf{Z}/\omega - \partial\mathbf{Z}/\partial\omega]\mathbf{V}/4. \tag{4}$$

Eqs. (3) and (4) require the system matrix and the velocity field of all elements. These hold for both undamped and damped systems. However, note that similar expressions with the corresponding mobility matrix ($\mathbf{M}$) and force vector ($\mathbf{F}$) in Eqs. (3) and (4) are not valid.

The corresponding energy formulation for a condensed version of Eqs. (3) and (4) is written as follows, where the subscript D implies the driving point:

$$\hat{\bar{E}}_{1Z,m} = \mathbf{V}_D^{*\mathrm{T}}\mathrm{Im}[\mathbf{Z}_D/\omega + \partial\mathbf{Z}_D/\partial\omega]\mathbf{V}_D/4, \tag{5}$$

$$\hat{\bar{E}}_{1Z,k} = -\mathbf{V}_D^{*\mathrm{T}}\mathrm{Im}[\mathbf{Z}_D/\omega - \partial\mathbf{Z}_D/\partial\omega]\mathbf{V}_D/4. \tag{6}$$

Here, the superscript $\hat{}$ denotes the energy estimate and the subscript $1Z$ indicates an estimate that is obtained by using Method 1 with impedance. Table 1 summarizes the subscripts that are used to denote the energy estimates in our article.

Similar procedure can be formulated with the mobility expression as follows where subscript $1M$ implies an estimate based on Method 1 with mobility:

$$\hat{\bar{E}}_{1M,m} = \mathbf{F}_D^{*\mathrm{T}}\mathrm{Im}[\mathbf{M}_D/\omega + \partial\mathbf{M}_D/\partial\omega]\mathbf{F}_D/4, \tag{7}$$

$$\hat{\bar{E}}_{1M,k} = -\mathbf{F}_D^{*\mathrm{T}}\mathrm{Im}[\mathbf{M}_D/\omega - \partial\mathbf{M}_D/\partial\omega]\mathbf{F}_D/4. \tag{8}$$

2.2. Method 2

In order to correct the improper occurrence of negative quantities from Method 1, Method 2 employs a correction factor $\alpha(\omega)$ to numerically compensate the error in $\hat{\bar{E}}_1$ [9]. Then, Method 2 adopts the following modified expression for the sum of kinetic and potential energies where subscript 2 indicates the estimate from Method 2 [9]:

$$[\hat{\bar{E}}_{2Z,m}(\omega) + \hat{\bar{E}}_{2Z,k}(\omega)] = [\hat{\bar{E}}_{1Z,m}(\omega) + \hat{\bar{E}}_{1Z,k}(\omega)]/\alpha_Z(\omega), \tag{9}$$

$$[\hat{\bar{E}}_{2M,m}(\omega) + \hat{\bar{E}}_{2M,k}(\omega)] = [\hat{\bar{E}}_{1M,m}(\omega) + \hat{\bar{E}}_{1M,k}(\omega)]/\alpha_M(\omega). \tag{10}$$

Table 1
Subscript symbols used to denote the energy estimates

Subscript	Method number	Subscript	Formulation type	Subscript	Energy type
1	Method 1 [8]	Z	Using impedance	m	Kinetic
2	Method 2 [9]			k	Potential
3	Method 3 [new]	M	Using mobility	d	Dissipation

Here, α_Z and α_M are calculated as follows where $\omega_{1,i}$ and $\omega_{2,i}$ are the first and second frequencies of the ith pair of zero crossing points in $\mathrm{Im}[\partial \mathbf{Z}_D/\partial\omega]$ and $\mathrm{Im}[\partial \mathbf{M}_D/\partial\omega]$ respectively:

$$\alpha(\omega) = \prod_i \left[\frac{(\omega-\omega_{0,i})^2 - (\Delta\omega_i)^2}{(\omega-\omega_{0,i})^2 + (\Delta\omega_i)^2}\right], \tag{11}$$

$$\omega_{0,i} = (\omega_{1,i} + \omega_{2,i})/2, \quad \Delta\omega_i = \omega_{2,i} - \omega_{1,i}/2. \tag{12,13}$$

It appears that α_Z and α_M model anti-resonances of $\mathrm{Im}[\partial \mathbf{Z}_D/\partial\omega]$ and $\mathrm{Im}[\partial \mathbf{M}_D/\partial\omega]$, respectively, by utilizing their zero-crossing points and to turn the negative values into positive ones and thus reduce errors. Although some improvements are seen in the numerical prediction with Method 2, the fundamental cause of the errors introduced by Methods 1 and 2 is still not well understood [8,9]. Therefore, the characterization scheme needs be carefully analyzed to understand its salient features and to seek possible improvements.

2.3. Comparative evaluation using a 3-dof example

The energy estimates with both impedance and mobility formulations are separately calculated for a three degree-of-freedom (3-dof) system of Fig. 1 where a sinusoidal force f_1 is applied to mass 1. Results are shown in Fig. 2 for a nominal set of system parameters where the damping loss factors are assumed as: $\eta_1 = \eta_{12} = \eta_{23} = \eta_3 = \eta$. It is observed that the estimates $(\hat{\bar{E}}_{1,m} + \hat{\bar{E}}_{1,k})$ with both impedance and mobility deviate from the exact energy spectra near resonances and anti-resonances. Further, Fig. 2 shows that the errors between the predicted and the exact energies increase as η increases. Furthermore, the mobility and impedance formulations yield different predictions, as compared in Fig. 2. It is also observed in Fig. 2 that Method 1 produces negative values for $\hat{\bar{E}}_{1,m} + \hat{\bar{E}}_{1,k}$ which correspond to $\mathrm{Im}[\partial \mathbf{Z}_D/\partial\omega]$ and $\mathrm{Im}[\partial \mathbf{M}_D/\partial\omega]$. Note that the sum of time-averaged kinetic and potential energies must be a positive quantity. Further note that negative values are not displayed in such logarithmic plots (Fig. 2 and subsequent) and thus the lines with the negative energy values are discontinuous at some frequencies.

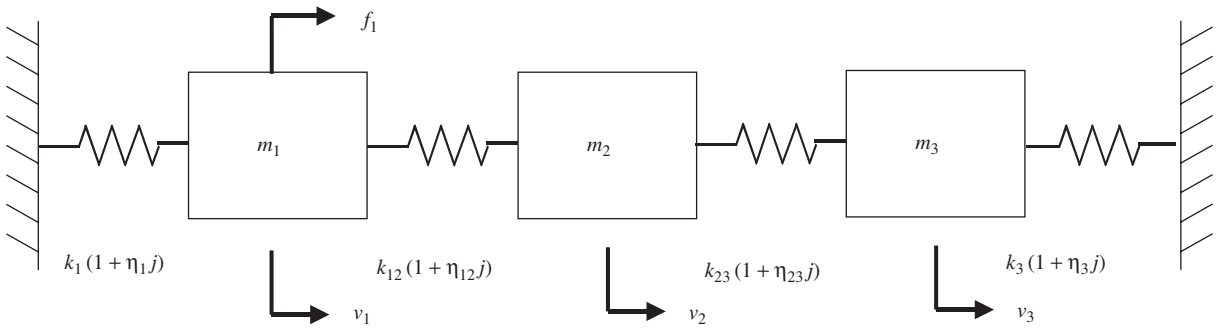

Fig. 1. Three dof system used to evaluate the energy characterization methods.

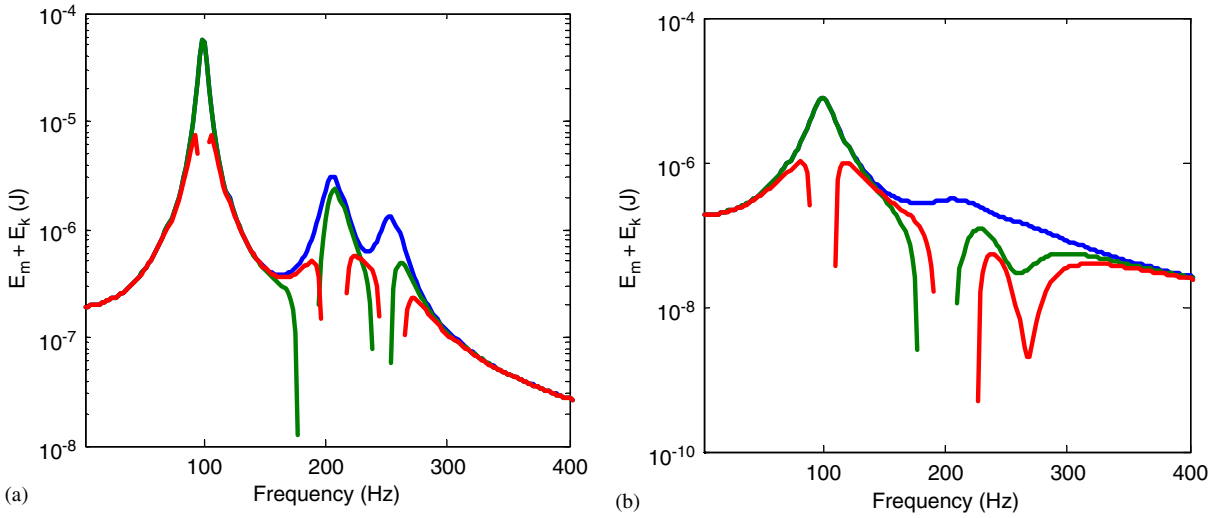

Fig. 2. Sum of time-averaged kinetic and potential energy estimates from Method 1 given a single sinusoidal force excitation to the system of Fig. 1: (a) lightly damped system ($\eta = 0.01$); (b) heavily damped system ($\eta = 0.2$). Key: ———, Exact; ———, estimate using impedance, ———, estimate using mobility.

Similar to Method 1, the energy estimates with Method 2 are calculated and results are shown in Fig. 3. It is observed in Fig. 3 that $\hat{\bar{E}}_{2,m}$ and $\hat{\bar{E}}_{2,k}$ are closer to the exact energies ($\bar{E}_m$ and $\bar{E}_k$) than the predictions from Method 1. However, $\hat{\bar{E}}_{2,m}$ and $\hat{\bar{E}}_{2,k}$ yet deviate from $\bar{E}_m$ and $\bar{E}_k$, and the deviations become more pronounced as η increases, like Method 1. For example, the negative values of $\hat{\bar{E}}_{2,k}$, that should not appear with the correction factor, are still observed for a highly damped system as shown in Fig. 3(d). This is because two resonances (around 200–300 Hz) are closely populated and the derivatives of impedance and mobility do not cross zeros at these frequencies. Hence, the correction process of Method 2 does not function well at these frequencies. Further, similar to Method 1, $\hat{\bar{E}}_{2,m}$ and $\hat{\bar{E}}_{2,k}$ via the mobility formulation differ from the estimates based on the impedance expressions. Moreover, spurious peaks are observed in $\hat{\bar{E}}_{2,m}$ and $\hat{\bar{E}}_{2,k}$ with both mobility and impedance formulations, as shown in Fig. 3. Further note that the kinetic energy deviates from the exact one at very low frequencies, say up to 20 Hz in this case.

3. Driving point transfer function and its derivative for a 2-dof model

3.1. Evaluation of Methods 1 and 2 using impedance formulation

In order to better understand the characterization schemes (5)–(8), a two degree-of-freedom (2-dof) model of Fig. 4 with a single harmonic force excitation at mass 1 is examined here. The equations of motion (in the frequency domain) are expressed as follows where $v_1 = |v_1|\phi_{v_1} e^{j\omega t}$,

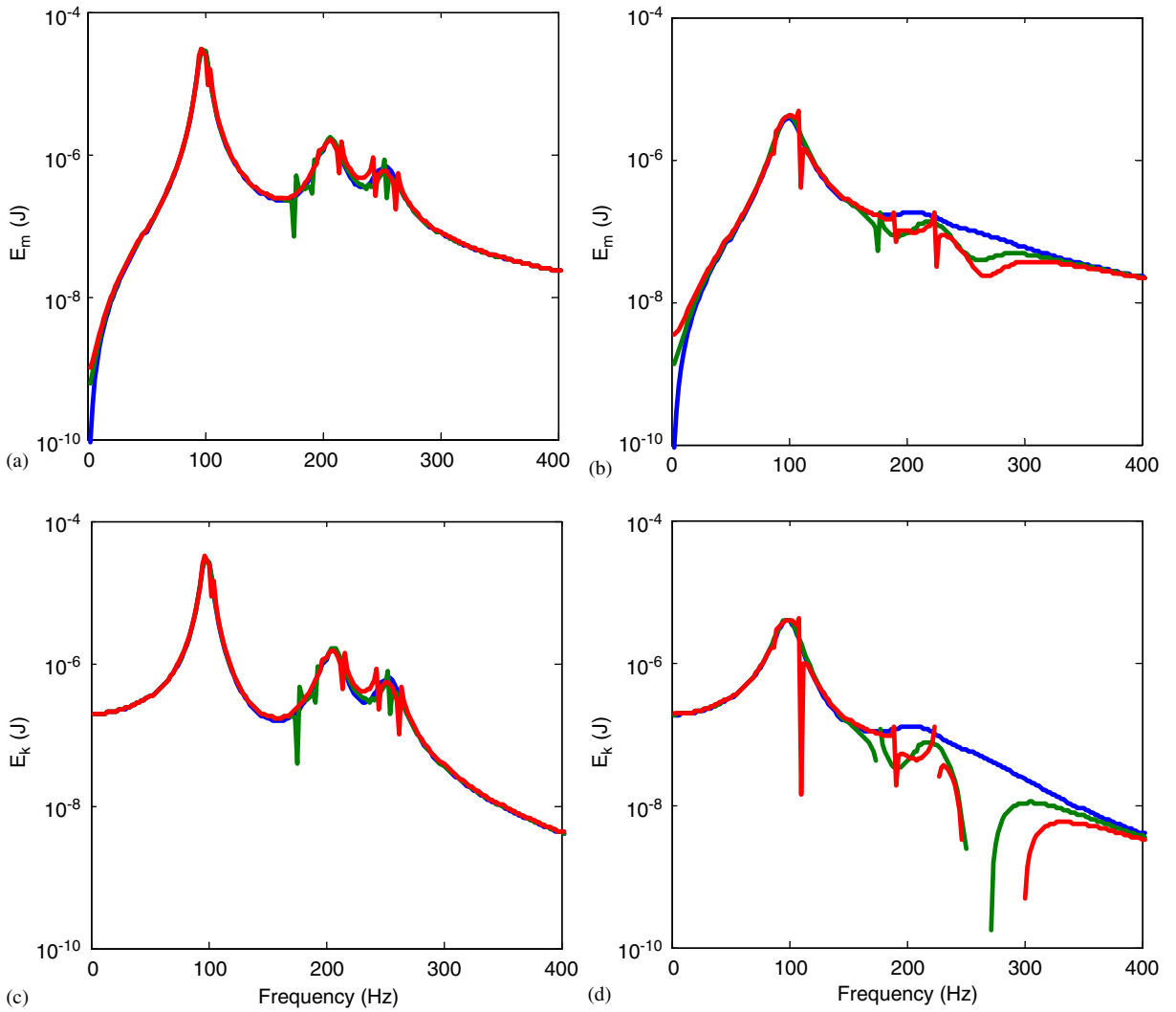

Fig. 3. Time-averaged energy estimates given a single sinusoidal force excitation to mass 1 of the system of Fig. 1: (a) Kinetic energy of a lightly damped system ($\eta = 0.01$); (b) kinetic energy of a heavily damped system ($\eta = 0.2$); (c) potential energy of a lightly damped system ($\eta = 0.01$); (d) potential energy of a heavily damped system ($\eta = 0.2$). Key: ——, Exact; ——, Method 2 estimate using impedance, ——, Method 2 estimate using mobility.

$v_2 = |v_2|\phi_{v_2} e^{j\omega t}$, $f_1 = |f_1|\phi_{f_1} e^{j\omega t}$ and z is the impedance:

$$z_{11}v_1 + z_{12}v_2 = f_1, \tag{14}$$

$$z_{21}v_1 + z_{22}v_2 = 0, \tag{15}$$

$$z_{11} = [j(m_1\omega - k_1/\omega) + k_1\eta_1/\omega], \quad z_{12} = -[-jk_{12}/\omega + k_{12}\eta_{12}/\omega], \tag{16,17}$$

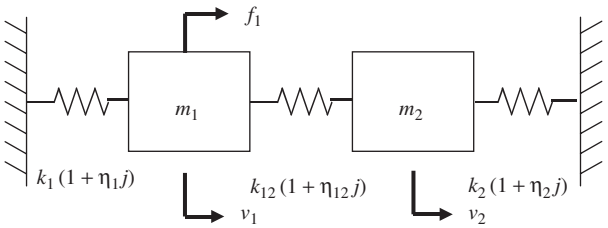

Fig. 4. 2-dof model used to evaluate Methods 1 and 2.

$$z_{21} = -[-\mathrm{j}k_{12}/\omega + k_{12}\eta_{12}/\omega], \tag{18}$$

$$z_{22} = [\mathrm{j}(m_2\omega - k_{12}/\omega - k_2/\omega) + k_{12}\eta_{12}/\omega + k_2\eta_2/\omega]. \tag{19}$$

Time-averaged kinetic, potential and dissipated energies of this system, respectively, are

$$\bar{E}_m = \tfrac{1}{2}\left[m_1|v_1|^2 + m_2|v_2|^2\right], \tag{20}$$

$$\bar{E}_k = \frac{1}{2}\left[\frac{k_1}{\omega^2}|v_1|^2 + \frac{k_{12}}{\omega^2}|v_1 - v_2|^2 + \frac{k_2}{\omega^2}|v_2|^2\right], \tag{21}$$

$$\bar{E}_d = \frac{1}{2}\left[\frac{\eta_1 k_1}{\omega^2}|v_1|^2 + \frac{\eta_{12}k_{12}}{\omega^2}|v_1 - v_2|^2 + \frac{\eta_2 k_2}{\omega^2}|v_2|^2\right]. \tag{22}$$

Consider the driving point impedance (z_{D11}). By using the relation $v_2 = -(z_{21}/z_{22})]v_1$ from Eq. (15), Eq. (14) is represented by z_{D11}, force and velocity at 1 as follows:

$$\left[z_{11} - z_{12}\frac{z_{21}}{z_{22}}\right]v_1 = z_{D11}v_1 = f_1. \tag{23}$$

Now, the energy predictions of Eqs. (5) and (6) based on Method 1 are expressed as follows by using the relationship $z_{12}/z_{22} = z_{21}/z_{22} = -v_2/v_1$:

$$v_1^* \frac{\partial z_{D11}}{\partial \omega} v_1 = v_1^* \left[\frac{\partial z_{11}}{\partial \omega} + \frac{\partial z_{12}}{\partial \omega}\frac{v_2}{v_1} + \frac{\partial z_{21}}{\partial \omega}\frac{v_2}{v_1} + \frac{\partial z_{22}}{\partial \omega}\left(\frac{v_2}{v_1}\right)^2\right] v_1. \tag{24}$$

On the other hand, the exact energy expression $[(\bar{E}_m + \bar{E}_k)\mathrm{j} - \bar{E}_d]$ is obtained as follows by substituting components of impedance matrix and velocity vector into the left-hand side of Eq. (2) and by using $v_2 = -(z_{21}/z_{22})]v_1$ since the energy description is valid with full impedance matrix and complete velocity field:

$$\mathbf{V}^{*\mathrm{T}}\left[\frac{\partial \mathbf{Z}}{\partial \omega}\right]\mathbf{V} = v_1^* \frac{\partial z_{D11}}{\partial \omega} v_1 = v_1^* \left[\frac{\partial z_{11}}{\partial \omega} - \frac{\partial z_{12}}{\partial \omega}\frac{z_{21}}{z_{22}} - \frac{\partial z_{21}}{\partial \omega}\frac{z_{12}^*}{z_{22}^*} + \frac{\partial z_{22}}{\partial \omega}\frac{z_{12}^*}{z_{22}^*}\frac{z_{21}}{z_{22}}\right] v_1. \tag{25}$$

Here, the $\partial z_{D11}/\partial\omega$ is defined as the "pseudo derivative" of z_{D11} with respect to ω. It is not available but it is still required to predict the correct energy description. Similar to the exact derivative, the "pseudo derivative" can be rewritten as

$$v_1^* \frac{\partial z_{D11}}{\partial \omega} v_1 = v_1^* \left[\frac{\partial z_{11}}{\partial \omega} + \frac{\partial z_{12}}{\partial \omega}\frac{v_2}{v_1} + \frac{\partial z_{21}}{\partial \omega}\left(\frac{v_2}{v_1}\right)^* + \frac{\partial z_{22}}{\partial \omega}\left|\frac{v_2}{v_1}\right|^2\right] v_1. \tag{26}$$

Now, compare the exact derivative $\partial z_{D11}/\partial\omega$ of Eq. (24) with the "pseudo derivative" $\partial z_{D11}/\partial\omega$ of Eq. (26). Observe that the difference between $\partial z_{D11}/\partial\omega$ and $\partial z_{D11}/\partial\omega$ arises because of the third and fourth terms of each equation. In other words, differences arise due to the opposite phase of impedance ratios z_{21}/z_{22} and z_{21}^*/z_{22}^*. Note that z_{21}/z_{22} and z_{12}/z_{22} correspond to velocity transmissibility (v_2/v_1) between the directly (v_1) and indirectly (v_2) excited dof. For an undamped system, $(z_{12}/z_{22}) = (z_{12}^*/z_{22}^*)$ or $(v_2/v_1) = (v_2^*/v_1^*)$ and then $\partial z_{D11}/\partial\omega$ is equal to $\partial z_{D11}/\partial\omega$. Further, substituting the derivatives of z components (16)–(19) into Eqs. (24) and (26), respectively, yields the following expressions:

$$v_1^* \frac{\partial z_{D11}}{\partial \omega} v_1 = v_1^* \left\{ \begin{array}{c} \mathrm{j}\left[m_1 + m_2 \left(\frac{v_2}{v_1}\right)^2 + \frac{k_1}{\omega^2} + \frac{k_{12}}{\omega^2}\left(\frac{v_1 - v_2}{v_1}\right)^2 + \frac{k_2}{\omega^2}\left(\frac{v_2}{v_1}\right)^2 \right] \\ -\frac{\eta_1 k_1}{\omega^2} - \frac{\eta_1 k_{12}}{\omega^2}\left(\frac{v_1 - v_2}{v_1}\right)^2 - \frac{\eta_1 k_2}{\omega^2}\left(\frac{v_2}{v_1}\right)^2 \end{array} \right\} v_1. \tag{27}$$

$$v_1^* \frac{\partial z_{D11}}{\partial \omega} v_1 = v_1^* \left\{ \begin{array}{c} \mathrm{j}\left[m_1 + m_2 \left|\frac{v_2}{v_1}\right|^2 + \frac{k_1}{\omega^2} + \frac{k_{12}}{\omega^2}\left|\frac{v_1 - v_2}{v_1}\right|^2 + \frac{k_2}{\omega^2}\left|\frac{v_2}{v_1}\right|^2 \right] \\ -\frac{\eta_1 k_1}{\omega^2} - \frac{\eta_1 k_{12}}{\omega^2}\left|\frac{v_1 - v_2}{v_1}\right|^2 - \frac{\eta_1 k_2}{\omega^2}\left|\frac{v_2}{v_1}\right|^2 \end{array} \right\} v_1. \tag{28}$$

Unlike Eq. (28) in the form of time-averaged energies, it is observed that the $\partial z_{D11}/\partial\omega$ of Eq. (27) consists of some form of energy relationship with a phase difference $(\Delta\phi_{2-1} = \phi_{v_2} - \phi_{v_1})$ between the driving point (v_1) and internal (v_2) dof. Multiply Eqs. (14) and (15), respectively, by v_1^* and v_2^* and sum the resulting two equations to yield the following well-known energy relationship:

$$v_1^* \frac{z_{D11}}{\omega} v_1 = v_1^* \left\{ \begin{array}{c} \mathrm{j}\left[m_1 + m_2 \left|\frac{v_2}{v_1}\right|^2 - \frac{k_1}{\omega^2} - \frac{k_{12}}{\omega^2}\left|\frac{v_1 - v_2}{v_1}\right|^2 - \frac{k_2}{\omega^2}\left|\frac{v_2}{v_1}\right|^2 \right] \\ +\frac{\eta_1 k_1}{\omega^2} + \frac{\eta_1 k_{12}}{\omega^2}\left|\frac{v_1 - v_2}{v_1}\right|^2 + \frac{\eta_1 k_2}{\omega^2}\left|\frac{v_2}{v_1}\right|^2 \end{array} \right\} v_1. \tag{29}$$

Now, substitute Eqs. (27) and (29) into Eqs. (5) and (6) to yield the energy estimates from Method 1 as follows:

$$\begin{aligned} \hat{\bar{E}}_{1Z,m} = {} & \frac{1}{2}\left[m_1 |v_1|^2 + \frac{1}{2} m_2 |v_2|^2 - \frac{1}{2}\frac{k_{12}}{\omega^2}|v_1 - v_2|^2 - \frac{1}{2}\frac{k_2}{\omega^2}|v_2|^2 \right] \\ & + \frac{1}{4}\mathrm{Re}\left\{ \left[m_2 (v_2)^2 + \frac{k_{12}}{\omega^2}(v_1 - v_2)^2 + \frac{k_2}{\omega^2}(v_2)^2 \right] \exp(-2j\phi_{v_1}) \right\} \\ & - \frac{1}{4}\mathrm{Im}\left\{ \left[\frac{\eta_1 k_{12}}{\omega^2}(v_1 - v_2)^2 + \frac{\eta_1 k_2}{\omega^2}(v_2)^2 \right] \exp(-2j\phi_{v_1}) \right\}. \end{aligned} \tag{30}$$

$$\hat{\bar{E}}_{1Z,k} = \frac{1}{2}\left[\frac{k_1}{\omega^2}|v_1|^2 + \frac{1}{2}\frac{k_{12}}{\omega^2}|v_1 - v_2|^2 + \frac{1}{2}\frac{k_2}{\omega^2}|v_2|^2 - \frac{1}{2}m_2|v_2|^2\right]$$
$$+ \frac{1}{4}\mathrm{Re}\left\{\left[m_2(v_2)^2 + \frac{k_{12}}{\omega^2}(v_1 - v_2)^2 + \frac{k_2}{\omega^2}(v_2)^2\right]\exp(-2\mathrm{j}\phi_{v_1})\right\}$$
$$- \frac{1}{4}\mathrm{Im}\left\{\left[\frac{\eta_1 k_{12}}{\omega^2}(v_1 - v_2)^2 + \frac{\eta_1 k_2}{\omega^2}(v_2)^2\right]\exp(-2j\phi_{v_1})\right\}. \quad (31)$$

Comparison of Eqs. (30) and (31) with Eqs. (20) and (21) shows that $\hat{\bar{E}}_{1Z,m}$ and $\hat{\bar{E}}_{1Z,k}$ deviate from $\bar{E}_m$ and $\bar{E}_k$, respectively. For example, $\hat{\bar{E}}_{1Z,m}$ consists not only of the kinetic energy but also of the potential and dissipated energies, as shown in Eq. (30). Likewise, Eq. (31) shows that $\hat{\bar{E}}_{1Z,k}$ contains other energies. For an undamped system, all elements are in the same phase and then $\hat{\bar{E}}_{1Z,m}$ of Eq. (30) and $\hat{\bar{E}}_{1Z,k}$ of Eq. (31) become equal to $\bar{E}_m$ and $\bar{E}_k$, respectively. Therefore, the energy prediction by Method 1 is valid only for an undamped (lossless) system and it should yield erroneous results for a damped structure. It is observed that both $\hat{\bar{E}}_{1Z,m}$ and $\hat{\bar{E}}_{1Z,k}$ may have negative values, unlike $\bar{E}_m$ and $\bar{E}_k$, since the second and third terms of Eqs. (30) and (31) may be negative. The difference between kinetic and potential energy components, as shown in the first terms of Eqs. (30) and (31), may also be negative. These negative values, which indicate an error in the estimates, are numerically converted into positive values via an "artificial" correction factor in Method 2 and thus some improvements in the estimates are found. Although the error is numerically compensated for in Method 2, both Methods 1 and 2 are still based on the same formulation and their inherent limitations still remain, as explained previously in Section 2.

3.2. Evaluation of mobility formulation

Now, the mobility formulation is considered and an exact derivative expression similar to Eq. (24) is

$$f_1^* \frac{\partial M_{D11}}{\partial \omega} f_1 = f_1^* \left[\frac{\partial Z_{D11}^{-1}}{\partial \omega}\right] f_1 = f_1^* \left[-M_{D11}\frac{\partial Z_{D11}}{\partial \omega} M_{D11}\right] f_1. \quad (32)$$

The left-hand side of Eq. (26) with the "pseudo" impedance that yields better estimates of Eqs. (5) and (6) is now extended to mobility as follows:

$$v_1^* \frac{\partial Z_{D11}}{\partial \omega} v_1 = f_1^* \left[M_{D11}^* \frac{\partial Z_{D11}}{\partial \omega} M_{D11}\right] f_1 = f_1^* \frac{\partial M_{D11}}{\partial \omega} f_1. \quad (33)$$

Like the impedance case, the $(\partial M_{D11})/\partial\omega$ of Eq. (26) is defined here as the "pseudo derivative" of mobility that produces the correct estimation along with the mobility formulation of Eqs. (7) and (8). A comparison of Eq. (32) with Eq. (33) shows that the exact derivative $(\partial M_{D11})/\partial\omega$ differs from $(\partial M_{D11})/\partial\omega$ and therefore the usage of $(\partial M_{D11})/\partial\omega$ with Eqs. (7) and (8) produces erroneous estimations.

4. General formulation for the derivatives of impedance or mobility

The aforementioned discussion can be generalized to a more than 2-dof system. The system equations are rewritten as follows where subscripts 1 and 2 denote directly and indirectly excited dof, respectively:

$$\mathbf{Z}_{11}\mathbf{V}_1 + \mathbf{Z}_{12}\mathbf{V}_2 = \mathbf{F}_1, \tag{34}$$

$$\mathbf{Z}_{21}\mathbf{V}_1 + \mathbf{Z}_{22}\mathbf{V}_2 = \mathbf{0}. \tag{35}$$

Like the 2-dof system case, the driving point impedance matrix is represented by sub-impedance matrices:

$$[\mathbf{Z}_{11} - \mathbf{Z}_{12}\mathbf{Z}_{22}^{-1}\mathbf{Z}_{21}]\mathbf{V}_1 = \mathbf{Z}_{D11}\mathbf{V}_1 = \mathbf{F}_1. \tag{36}$$

The exact derivative of $\mathbf{Z}_{D11}$ with respect to frequency is

$$\frac{\partial \mathbf{Z}_{D11}}{\partial \omega} = \frac{\partial \mathbf{Z}_{11}}{\partial \omega} - \frac{\partial \mathbf{Z}_{12}}{\partial \omega}\mathbf{Z}_{22}^{-1}\mathbf{Z}_{21} - \mathbf{Z}_{21}^{\mathrm{T}}\mathbf{Z}_{22}^{-1^{\mathrm{T}}}\frac{\partial \mathbf{Z}_{21}}{\partial \omega} + \mathbf{Z}_{21}^{\mathrm{T}}\mathbf{Z}_{22}^{-1^{\mathrm{T}}}\frac{\partial \mathbf{Z}_{22}}{\partial \omega}\mathbf{Z}_{22}^{-1}\mathbf{Z}_{21}. \tag{37}$$

Similar to Eq. (25), the "pseudo derivative" of $\mathbf{Z}_{D11}$ with respect to ω that correctly describes the energy distribution is expressed as follows:

$$\frac{\partial \mathbf{Z}_{D11}}{\partial \omega} = \frac{\partial \mathbf{Z}_{11}}{\partial \omega} - \frac{\partial \mathbf{Z}_{12}}{\partial \omega}\mathbf{Z}_{22}^{-1}\mathbf{Z}_{21} - \mathbf{Z}_{21}^{*\mathrm{T}}\mathbf{Z}_{22}^{*-1^{\mathrm{T}}}\frac{\partial \mathbf{Z}_{21}}{\partial \omega} + \mathbf{Z}_{21}^{*\mathrm{T}}\mathbf{Z}_{22}^{*-1^{\mathrm{T}}}\frac{\partial \mathbf{Z}_{22}}{\partial \omega}\mathbf{Z}_{22}^{-1}\mathbf{Z}_{21}. \tag{38}$$

Like Eqs. (27)–(29), detailed energies of $\partial \mathbf{Z}_{D11}/\partial\omega$, $\partial \mathbf{Z}_{D11}/\partial\omega$ and $\mathbf{Z}_{D11}/\omega$ are described for a single excitation case as follows where i is the dof index:

$$v_1^* \frac{\partial z_{D11}}{\partial \omega} v_1 = v_1^* \left\{ \begin{array}{c} \mathrm{j}\left[\sum_i m_i \left(\frac{v_i}{v_1}\right)^2 + \frac{1}{2}\sum_i \sum_j \frac{k_{ij}}{\omega^2}\left(\frac{v_i - v_j}{v_1}\right)^2 + \sum_i \frac{k_i}{\omega^2}\left(\frac{v_i}{v_1}\right)^2 \right] \\ -\frac{1}{2}\sum_i \sum_j \frac{\eta_{ij}k_{ij}}{\omega^2}\left(\frac{v_i - v_j}{v_1}\right)^2 - \sum_i \frac{\eta_i k_i}{\omega^2}\left(\frac{v_i}{v_1}\right)^2 \end{array} \right\} v_1, \tag{39}$$

$$v_1^* \frac{\partial z_{D11}}{\partial \omega} v_1 = v_1^* \left\{ \begin{array}{c} \mathrm{j}\left[\sum_i m_i \left|\frac{v_i}{v_1}\right|^2 + \frac{1}{2}\sum_i \sum_j \frac{k_{ij}}{\omega^2}\left|\frac{v_i - v_j}{v_1}\right|^2 + \sum_i \frac{k_i}{\omega^2}\left|\frac{v_i}{v_1}\right|^2 \right] \\ -\frac{1}{2}\sum_i \sum_j \frac{\eta_{ij}k_{ij}}{\omega^2}\left|\frac{v_i - v_j}{v_1}\right|^2 - \sum_i \frac{\eta_i k_i}{\omega^2}\left|\frac{v_i}{v_1}\right|^2 \end{array} \right\} v_1, \tag{40}$$

$$v_1^* \frac{z_{D11}}{\omega} v_1 = v_1^* \left\{ \begin{array}{c} \mathrm{j}\left[\sum_i m_i \left|\frac{v_i}{v_1}\right|^2 - \frac{1}{2}\sum_i \sum_j \frac{k_{ij}}{\omega^2}\left|\frac{v_i - v_j}{v_1}\right|^2 - \sum_i \frac{k_i}{\omega^2}\left|\frac{v_i}{v_1}\right|^2 \right] \\ +\frac{1}{2}\sum_i \sum_j \frac{\eta_{ij}k_{ij}}{\omega^2}\left|\frac{v_i - v_j}{v_1}\right|^2 + \sum_i \frac{\eta_i k_i}{\omega^2}\left|\frac{v_i}{v_1}\right|^2 \end{array} \right\} v_1. \tag{41}$$

By substituting Eqs. (39) and (31) into Eqs. (5) and (6), respectively, $\hat{\tilde{E}}_{1Z,m}$ and $\hat{\tilde{E}}_{1Z,k}$ can be derived. These would produce errors, such as Eqs. (30) and (31). Similarly, the actual and

"pseudo" derivatives of mobility and detailed energies with mobility are expressed as follows and substituting these into Eqs. (7) and (8) also would yield erroneous results as shown in Fig. 2:

$$\frac{\partial \mathbf{M}_{D11}}{\partial \omega} = -\mathbf{M}_{D11}\frac{\partial \mathbf{Z}_{D11}}{\partial \omega}\mathbf{M}_{D11}, \quad \frac{\partial \mathbf{M}_{D11}}{\partial \omega} = \mathbf{M}_{D11}^{*\mathrm{T}}\frac{\partial \mathbf{Z}_{D11}}{\partial \omega}\mathbf{M}_{D11}. \tag{42a,b}$$

$$f_1^*\frac{\partial M_{D11}}{\partial \omega}f_1 = |f_1|^2\left\{\begin{array}{c} \mathrm{j}\left[\sum_i m_i\left(\frac{v_i}{f_1}\right)^2 + \frac{1}{2}\sum_i\sum_j \frac{k_{ij}}{\omega^2}\left(\frac{v_i - v_j}{f_1}\right)^2 + \sum_i \frac{k_i}{\omega^2}\left(\frac{v_i}{f_1}\right)^2\right] \\ -\frac{1}{2}\sum_i\sum_j \frac{\eta_{ij}k_{ij}}{\omega^2}\left(\frac{v_i - v_j}{f_1}\right)^2 - \sum_i \frac{\eta_i k_i}{\omega^2}\left(\frac{v_i}{f_1}\right)^2 \end{array}\right\}, \tag{43}$$

$$f_1^*\frac{\partial M_{D11}}{\partial \omega}f_1 = |f|^2\left\{\begin{array}{c} \mathrm{j}\left[\sum_i m_i\left|\frac{v_i}{f_1}\right|^2 + \frac{1}{2}\sum_i\sum_j \frac{k_{ij}}{\omega^2}\left|\frac{v_i - v_j}{f_1}\right|^2 + \sum_i \frac{k_i}{\omega^2}\left|\frac{v_i}{f_1}\right|^2\right] \\ -\frac{1}{2}\sum_i\sum_j \frac{\eta_{ij}k_{ij}}{\omega^2}\left|\frac{v_i - v_j}{f_1}\right|^2 - \sum_i \frac{\eta_i k_i}{\omega^2}\left|\frac{v_i}{f_1}\right|^2 \end{array}\right\}. \tag{44}$$

5. New spectral energy formulation (Method 3)

In order to better understand and properly utilize the frequency derivative of transfer functions, consider Eq. (39) and note that $\partial z_{D11}/\partial\omega$ consists of an oscillating energy component with 2ω frequency rather than the time-averaged energy.

Instantaneous kinetic energies of a system are summed below where each element has the velocity of $v_i(t;\omega) = V_i\cos(\omega t + \phi_{v_i})$:

$$E_m(t;\omega) = \sum_i \frac{1}{2}m_i v_i^2 = \sum_i \frac{1}{2}m_i V_i^2\cos^2(\omega t + \phi_{v_i}) = \bar{E}_m(t;\omega) + \tilde{E}_m(t;\omega), \tag{45}$$

$$\bar{E}_m(t;\omega) = \sum_i \frac{1}{4}m_i V_i^2, \quad \tilde{E}_m(t;\omega) = \sum_i \frac{1}{4}m_i V_i^2\cos(2\omega t + 2\phi_{v_i}), \tag{46,47}$$

The instantaneous potential and dissipated energies can be expressed in a similar manner. Next, the spectral energies of a system (at frequency ω) are defined as follows where $v_i^2 = |v_i|^2\exp[\mathrm{j}(2\omega + 2\phi_{v_i})]$:

$$\tilde{E}_m(\omega) = \left|\tilde{E}_m\right|\exp[\mathrm{j}(2\omega + \phi_{\tilde{E}_m})] = \frac{1}{2}\sum_i m_i v_i^2, \tag{48}$$

$$\tilde{E}_k(\omega) = \left|\tilde{E}_k\right|\exp[\mathrm{j}(2\omega + \phi_{\tilde{E}_k})] = -\frac{1}{2}\sum_i\left[\frac{k_i}{\omega^2}v_i^2 + \frac{1}{2}\sum_j \frac{k_{ij}}{\omega^2}(v_i - v_j)^2\right], \tag{49}$$

$$\tilde{E}_d(\omega) = \left|\tilde{E}_d\right| \exp[\mathrm{j}(2\omega + \phi_{\tilde{E}_d})] = -\frac{1}{2}\sum_i \left[\frac{\eta_i k_i}{\omega^2} v_i^2 + \frac{1}{2}\sum_j \frac{\eta_{ij} k_{ij}}{\omega^2}\left(v_i - v_j\right)^2\right]. \tag{50}$$

Here, $\tilde{E}_m$, $\tilde{E}_k$ and $\tilde{E}_d$ are the complex-valued kinetic, potential and dissipated energy components, respectively. Further, note that the negative sign is imposed on the right-hand side of Eqs. (49) and (50) to preserve the potential and dissipated energy definitions, that is, $k_i x_i^2 = -(k_i/\omega^2)v_i^2$ and $\eta_i k_i x_i^2 = -\eta_i (k_i/\omega^2) v_i^2$.

Then, the $\partial z_{D11}/\partial\omega$ is rewritten as follows:

$$\frac{1}{2}\frac{\partial z_{D11}}{\partial \omega} = \mathrm{j}\left[\frac{\tilde{E}_m}{v_1^2} - \frac{\tilde{E}_k}{v_1^2}\right] + \frac{\tilde{E}_d}{v_1^2}. \tag{51}$$

Multiplying Eq. (51) by v_1^2 yields the following:

$$\frac{1}{2} v_1 \frac{\partial z_{D11}}{\partial \omega} v_1 = \mathrm{j}\left[\tilde{E}_m - \tilde{E}_k\right] + \tilde{E}_d. \tag{52}$$

Like the energy relation (41) for z_{D11}/ω, the following expression is also valid and is obtained by multiplying Eqs. (14) and (15) by v_1 and v_2, respectively, and summing the two equations:

$$\frac{1}{2} v_1 \frac{z_{D11}}{\omega} v_1 = \mathrm{j}\left[\tilde{E}_m + \tilde{E}_k\right] - \tilde{E}_d. \tag{53}$$

Similar to procedure (3) and (4) for $\bar{E}$, the following formulation predicts the spectral energies $\tilde{E}$ with the driving point impedance and its derivative:

$$\tilde{E}_{Z,m} = \frac{1}{4\mathrm{j}} v_1 \left[\frac{z_{D11}}{\omega} + \frac{\partial z_{D11}}{\partial \omega}\right] v_1, \tag{54}$$

$$\tilde{E}_{Z,k} + \mathrm{j}\tilde{E}_{Z,d} = \frac{1}{4\mathrm{j}} v_1 \left[\frac{z_{D11}}{\omega} - \frac{\partial z_{D11}}{\partial \omega}\right] v_1. \tag{55}$$

Assuming the damping loss factor is small (say $\eta < 0.2$), $\tilde{E}_{Z,k}$ is approximated as follows:

$$\tilde{E}_{Z,k} \approx \frac{1}{4\mathrm{j}} v_1 \left[\frac{z_{D11}}{\omega} - \frac{\partial z_{D11}}{\partial \omega}\right] v_1 \quad \text{for} \quad \tilde{E}_{Z,k} \gg \tilde{E}_{Z,d}. \tag{56}$$

Represent $\tilde{E}_m$ and $\bar{E}_m$ as follows, where $v_i = \mathrm{Re}(v_i) + \mathrm{Im}(v_i)$:

$$\bar{E}_m = \frac{1}{2}\sum_i m_i \left[[\mathrm{Re}(v_i)]^2 + [\mathrm{Im}(v_i)]^2\right], \tag{57}$$

$$\tilde{E}_m = \frac{1}{2}\left[\sum_i m_i \left[[\mathrm{Re}(v_i)]^2 - [\mathrm{Im}(v_i)]^2\right] + \mathrm{j}\sum [2 m_i \mathrm{Re}(v_i)\cdot \mathrm{Im}(v_i)]\right]. \tag{58}$$

Further describe $|\tilde{E}_m|$ as

$$|\tilde{E}_m| = \frac{1}{2}\left[\begin{array}{c}\left[\sum_i m_i[\mathrm{Re}(v_i)]^2\right]^2 + \left[\sum_i m_i[\mathrm{Im}(v_i)]^2\right]^2 \\ -2\left[\sum_i m_i[\mathrm{Re}(v_i)]^2\right]\left[\sum_i m_i[\mathrm{Im}(v_i)]^2\right] + 4\left[\sum_i m_i[\mathrm{Re}(v_i)\cdot\mathrm{Im}(v_i)]\right]^2\end{array}\right]^{1/2}. \quad (59)$$

Then, $\bar{E}_m$ may be approximated as

$$\bar{E}_m \approx |\tilde{E}_m|, \quad (60)$$

$$\text{when} \quad \left[\sum_i m_i[\mathrm{Re}(v_i)]^2\right]\left[\sum_i m_i[\mathrm{Im}(v_i)]^2\right] = \left[\sum_i m_i[\mathrm{Re}(v_i)\cdot\mathrm{Im}(v_i)]\right]^2. \quad (61)$$

An undamped system meets the condition of Eq. (61) since the imaginary part of v_i does not exist and both sides of Eq. (61) are equal to zero. Similar to $\bar{E}_m$, $\bar{E}_k$ is approximated as follows where only the first term on the right-hand side of Eq. (49) is expressed here for the sake of explanation:

$$\bar{E}_k \approx |\tilde{E}_k|, \quad \text{when} \quad \left[\sum_i \frac{k_i}{\omega^2}[\mathrm{Re}(v_i)]^2\right]\left[\sum_i \frac{k_i}{\omega^2}[\mathrm{Im}(v_i)]^2\right] = \left[\sum_i \frac{k_i}{\omega^2}[\mathrm{Re}(v_i)\cdot\mathrm{Im}(v_i)]\right]^2. \quad (62,63)$$

The approximations given by Eqs. (60)–(63) are designated here as Method 3. The energy estimates from Method 3 are therefore:

$$\hat{\bar{E}}_{3Z,m} = |\tilde{E}_{Z,m}|, \quad \hat{\bar{E}}_{3Z,k} = |\tilde{E}_{Z,k}|. \quad (64,65)$$

Time-averaged dissipated energy can be calculated by using the well-known vibratory power flow theory [3]. Time-averaged dissipated energy is

$$\begin{aligned}\bar{E}_d &= \frac{1}{2\omega}\mathrm{Re}[v(\omega)\cdot f^*(\omega)] = \frac{1}{2\omega}\mathrm{Re}[f(\omega)\cdot v^*(\omega)] \\ &= \frac{1}{2\omega}|f(\omega)|^2\mathrm{Re}[M] = \frac{1}{2\omega}|v(\omega)|^2\mathrm{Re}[Z].\end{aligned} \quad (66)$$

The system of Fig. 1 is re-analyzed to examine Method 3 and the calculated results are shown in Fig. 5. Observe that Method 3 predicts values that are closer to the exact energies. Unlike Method 2, Method 3 produces consistent predictions from impedance or mobility. The spurious peaks, which result due to the numerical modeling process of Method 2, do not appear in the estimates of Method 3. Furthermore, $\hat{\bar{E}}_{3,m}$ yields almost exact values, unlike Method 2, at lower frequencies. However, the estimates of Method 3 show some deviations from exact energies near the second and third resonances for a highly damped system, as observed in Fig. 5.

6. Spectral energies of one-dimensional continuous structure

Next, we apply Methods 2 and 3 to a one-dimensional continuous structure. A clamped–free beam of Fig. 6 is considered to examine the energy measures and characterization methods.

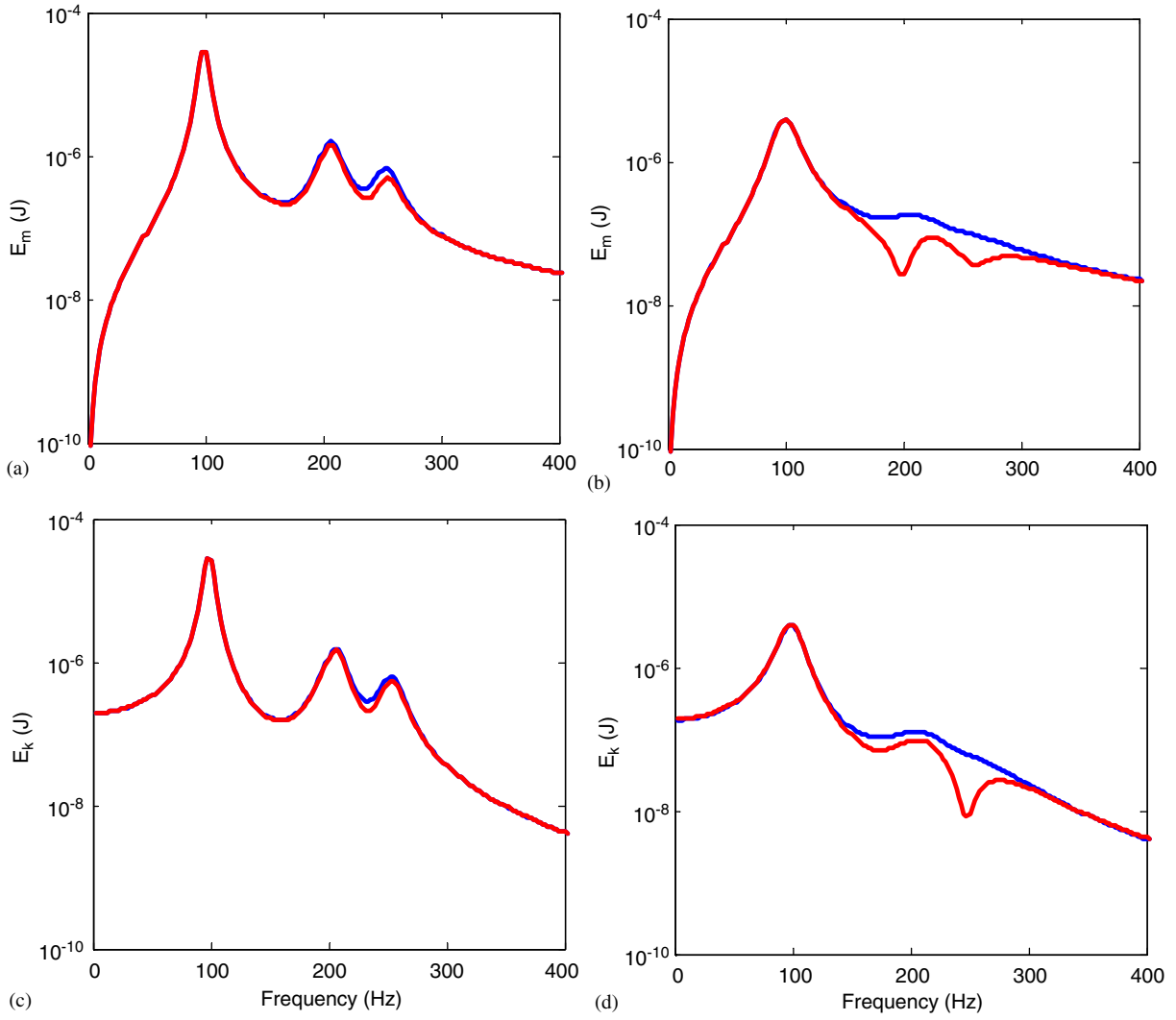

Fig. 5. Time-averaged energy estimates given a force excitation at mass 1 for the system of Fig. 1: (a) kinetic energy of a lightly damped system ($\eta = 0.01$); (b) kinetic energy of a heavily damped system ($\eta = 0.2$); (c) potential energy of a lightly damped system ($\eta = 0.01$); (d) potential energy of a heavily damped system ($\eta = 0.2$). Key: ——, Exact; ——, Method 3 using impedance or mobility.

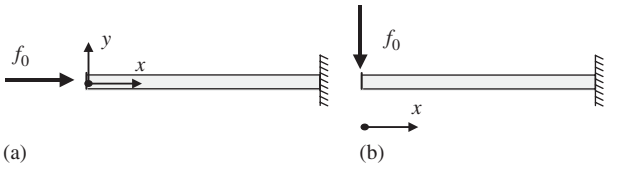

Fig. 6. Clamped–free beam given a sinusoidal force excitation at the free edge ($x = 0$): (a) under longitudinal excitation; (b) under flexural excitation.

Longitudinal and flexural motions are separately examined by applying a harmonic force (of amplitude f_0) to the free end (at $x = 0$) in the corresponding directions, as shown in Fig. 6(a) and 6(b), respectively.

6.1. Longitudinal motions

Velocity amplitude (v) of the clamped–free beam given a harmonic force of amplitude f_0 is written as follows where ρ, S and L are the mass density, the section area and the length of the beam, respectively:

$$v(x;\omega) = \frac{f_0\omega}{S\tilde{\mathrm{E}}\kappa_L}\frac{[\exp(\mathrm{j}\tilde{\kappa}_L x) - \exp(-\mathrm{j}\tilde{\kappa}_L x)]}{[\exp(\mathrm{j}\tilde{\kappa}_L L) + \exp(-\mathrm{j}\tilde{\kappa}_L L)]}. \tag{67}$$

Here, $\tilde{\mathrm{E}}$ and κ_L represent the complex modulus and the longitudinal wavenumber, respectively, and are expressed as follow where superscripts $'$ and $''$ denote the real and imaginary parts, respectively:

$$\tilde{\mathrm{E}}(\omega) = \mathrm{E}'(1+\mathrm{j}\eta) = \mathrm{E}' + \mathrm{j}\mathrm{E}'',\ \tilde{\kappa}_L = \omega\sqrt{\rho/\tilde{\mathrm{E}}} = \kappa_L' + \mathrm{j}\kappa_L'' \approx \omega\sqrt{\rho/\mathrm{E}'}\left[(1 - \mathrm{j}\eta/2)\right]. \tag{68,69}$$

The squared-magnitude of velocity is

$$\begin{aligned}\left|v(x;\omega)\right|^2 &= v(x)\cdot v^*(x)\\ &= \frac{\omega^2\left|f_0\right|^2\left[\exp(-2\kappa_L'' x) + \exp(2\kappa_L'' x) - \exp(2\mathrm{j}\kappa_L' x) - \exp(-2\mathrm{j}\kappa_L' x)\right]}{S^2\left|\tilde{\mathrm{E}}\right|^2|\tilde{\kappa}_L|\left|\exp(\mathrm{j}\tilde{\kappa}_L L) + \exp(-\mathrm{j}\tilde{\kappa}_L L)\right|^2}.\end{aligned} \tag{70}$$

Time-averaged kinetic energy within the finite beam at frequency ω is expressed as

$$\begin{aligned}\bar{E}_m &= \frac{\rho S}{2}\int_0^L \left|v(x)\right|^2 \mathrm{d}x\\ &= \frac{\left|f_0\right|^2\kappa_L'\left[\left[\exp(2\kappa_L'' x) - \exp(-2\kappa_L'' x)\right] + \mathrm{j}\kappa_L''\left[\exp(2\mathrm{j}\kappa_L' x) - \exp(-2\mathrm{j}\kappa_L' x)\right]\right]}{4S\left|\tilde{\mathrm{E}}\right|\left|\exp(\mathrm{j}\tilde{\kappa}_L L) + \exp(-\mathrm{j}\tilde{\kappa}_L L)\right|^2\kappa_L''\kappa_L'}.\end{aligned} \tag{71}$$

The gradient of displacement (ξ) and the square of its amplitude are expressed below:

$$\frac{\partial\xi(x)}{\partial x} = \frac{-\mathrm{j}f_0}{S\tilde{\mathrm{E}}}\frac{[\exp(\mathrm{j}\tilde{\kappa}_L x) + \exp(-\mathrm{j}\tilde{\kappa}_L x)]}{[\exp(\mathrm{j}\tilde{\kappa}_L L) + \exp(-\mathrm{j}\tilde{\kappa}_L L)]}, \tag{72}$$

$$\begin{aligned}\left|\frac{\partial\xi(x)}{\partial x}\right|^2 &= \frac{\partial\xi(x)}{\partial x}\cdot\left[\frac{\partial\xi(x)}{\partial x}\right]^*\\ &= \frac{\left|f_0\right|^2\left[\exp(-2\kappa_L'' x) + \exp(2\kappa_L'' x) + \exp(2\mathrm{j}\kappa_L' x) + \exp(-2\mathrm{j}\kappa_L' x)\right]}{S^2\left|\tilde{\mathrm{E}}\right|^2\left|\exp(\mathrm{j}\tilde{\kappa}_L L) + \exp(-\mathrm{j}\tilde{\kappa}_L L)\right|^2}.\end{aligned} \tag{73}$$

Time-averaged potential and dissipated energies within the finite beam are derived as follows:

$$\bar{E}_k(\omega) = \frac{S\mathrm{E}'}{2}\int_0^\infty \left|\frac{\partial\xi(x)}{\partial x}\right|^2 \mathrm{d}x = \frac{\mathrm{E}'|f_0|^2\left[\kappa'_L\left[\exp(2\kappa''_L x)-\exp(-2\kappa''_L x)\right]-\mathrm{j}\kappa''_L\left[\exp(2\mathrm{j}\kappa'_L x)-\exp(-2\mathrm{j}\kappa'_L x)\right]\right]}{4S|\tilde{\mathrm{E}}|^2\left|\exp(\mathrm{j}\tilde{\kappa}_L L)+\exp(-\mathrm{j}\tilde{\kappa}_L L)\right|^2\kappa''_L\kappa'_L}, \tag{74}$$

$$\bar{E}_d(\omega) = \frac{S\mathrm{E}''}{2}\int_0^\infty \left|\frac{\partial\xi(x)}{\partial x}\right|^2 \mathrm{d}x = \frac{\mathrm{E}''|f_0|^2\left[\kappa'_L\left[\exp(2\kappa''_L x)-\exp(-2\kappa''_L x)\right]-\mathrm{j}\kappa''_L\left[\exp(2\mathrm{j}\kappa'_L x)-\exp(-2\mathrm{j}\kappa'_L x)\right]\right]}{4S|\tilde{\mathrm{E}}|^2\left|\exp(\mathrm{j}\tilde{\kappa}_L L)+\exp(-\mathrm{j}\tilde{\kappa}_L L)\right|^2\kappa''_L\kappa'_L}. \tag{75}$$

Finally, the $\bar{E}_d$ expression can also be obtained from the vibration power formulation (66).

6.2. Flexural motions

Next, flexural motions of a clamped-free beam are considered and the flexural velocity field is

$$v(x;\omega) = \frac{\mathrm{j}\omega f_0[A\exp(\mathrm{j}\tilde{\kappa}_B x)+B\exp(-\mathrm{j}\tilde{\kappa}_B x)+C\exp(\tilde{\kappa}_B x)+D\exp(-\tilde{\kappa}_B x)]}{-2\tilde{\mathrm{E}}I\tilde{\kappa}_B^3[\cos(\tilde{\kappa}_B L)\cosh(\tilde{\kappa}_B L)+1]}, \tag{76}$$

$$A = \left\{[\sin(\tilde{\kappa}_B L)+\sinh(\tilde{\kappa}_B L)]+\mathrm{j}[\cos(\tilde{\kappa}_B L)+\cosh(\tilde{\kappa}_B L)]\right\}/2, \tag{77}$$

$$B = \left\{[\sin(\tilde{\kappa}_B L)+\sinh(\tilde{\kappa}_B L)]-\mathrm{j}[\cos(\tilde{\kappa}_B L)+\cosh(\tilde{\kappa}_B L)]\right\}/2, \tag{78}$$

$$C = \left\{-[\sin(\tilde{\kappa}_B L)+\sinh(\tilde{\kappa}_B L)]+\mathrm{j}[\cos(\tilde{\kappa}_B L)+\cosh(\tilde{\kappa}_B L)]\right\}/2, \tag{79}$$

$$D = \left\{-[\sin(\tilde{\kappa}_B L)+\sinh(\tilde{\kappa}_B L)]-\mathrm{j}[\cos(\tilde{\kappa}_B L)+\cosh(\tilde{\kappa}_B L)]\right\}/2. \tag{80}$$

Here, I is the area moment of inertia and the following $\tilde{\kappa}_B$ represent the complex flexural wavenumber where superscripts $'$ and $''$ denote the real and imaginary parts, respectively:

$$\tilde{\kappa}_B = \sqrt[4]{\omega^2\rho S/\tilde{\mathrm{E}}I} = \kappa'_B + \mathrm{j}\kappa''_B \approx \sqrt[4]{\omega^2\rho S/I\mathrm{E}'}\left[(1-\mathrm{j}\eta/4)\right]. \tag{81}$$

After a lengthy manipulation, the square of velocity amplitude is derived as

$$|v(x;\omega)|^2 = v(x)\cdot v(x)^* = Q_1\left[\frac{\omega^2|f_0|^2}{4|\tilde{\mathrm{E}}|^2 I^2|\tilde{\kappa}_B|^6\left|\cos(\tilde{\kappa}_B L)\cosh(\tilde{\kappa}_B L)+1\right|^2}\right], \tag{82}$$

$$Q_1 = \begin{bmatrix} |A|^2\exp(-2\kappa''_B x)+|B|^2\exp(2\kappa''_B x)+|C|^2\exp(2\kappa'_B x)+|D|^2\exp(-2\kappa'_B x) \\ +2\cdot\mathrm{Re}\begin{bmatrix} AB^*\exp(2\mathrm{j}\kappa'_B x)+CD^*\exp(2\mathrm{j}\kappa''_B x) \\ +AC^*\exp[(\kappa'_B-\kappa''_B)(1+\mathrm{j})x]+AD^*\exp[(\kappa'_B+\kappa''_B)(-1+\mathrm{j})x] \\ +BC^*\exp[(\kappa'_B+\kappa''_B)(1-\mathrm{j})x]+BD^*\exp[(-\kappa'_B+\kappa''_B)(1+\mathrm{j})x] \end{bmatrix} \end{bmatrix}. \tag{83}$$

Time-averaged kinetic energy is obtained as follows by integrating $|v(x)^2|$ over the finite beam span ($x = 0$ to l):

$$\bar{E}_m(\omega) = \frac{\rho S}{2}\int_0^L \left|v(x)\right|^2 \mathrm{d}x = [Q_2 + Q_3]\left[\frac{\rho S\omega^2\left|f_0\right|^2}{8\left|\tilde{\mathrm{E}}\right|^2 I^2|\tilde{\kappa}_B|^6\left|\cos(\tilde{\kappa}_B L)\cosh(\tilde{\kappa}_B L)+1\right|^2}\right], \tag{84}$$

$$\begin{aligned} Q_2 = & -|A|^2\left[\exp(-2\kappa''_B L)-1\right]/(2\kappa''_B) + |B|^2\left[\exp(2\kappa''_B L)-1\right]/(2\kappa''_B) \\ & + |C|^2\left[\exp(2\kappa'_B L)-1\right]/(2\kappa'_B) - |D|^2\left[\exp(-2\kappa'_B L)-1\right]/(2\kappa'_B), \end{aligned} \tag{85}$$

$$Q_3 = 2\cdot\mathrm{Re}\begin{bmatrix} AB^*\left[\exp(2\mathrm{j}\kappa'_B L)-1\right]/(2\mathrm{j}\kappa'_B) + CD^*\left[\exp(2\mathrm{j}\kappa''_B L)-1\right]/(2\mathrm{j}\kappa''_B) \\ +AC^*\left[\exp((\kappa'_B-\kappa''_B)(1+\mathrm{j})L)-1\right]/((\kappa'_B-\kappa''_B)(1+\mathrm{j})) \\ +AD^*\left[\exp((\kappa'_B+\kappa''_B)(-1+\mathrm{j})L)-1\right]/((\kappa'_B+\kappa''_B)(-1+\mathrm{j})) \\ +BC^*\left[\exp((\kappa'_B+\kappa''_B)(1-\mathrm{j})L)-1\right]/((\kappa'_B+\kappa''_B)(1-\mathrm{j})) \\ +BD^*\left[\exp((-\kappa'_B+\kappa''_B)(1+\mathrm{j})L)-1\right]/((-\kappa'_B+\kappa''_B)(1+\mathrm{j})) \end{bmatrix}. \tag{86}$$

Displacement and its second derivative with respect to the longitudinal coordinate (x) are

$$\xi(x) = \frac{f_0[A\exp(\mathrm{j}\tilde{\kappa}_B x) + B\exp(-\mathrm{j}\tilde{\kappa}_B x) + C\exp(\tilde{\kappa}_B x) + D\exp(-\tilde{\kappa}_B x)]}{-2\tilde{\mathrm{E}}I\tilde{\kappa}_B^3[\cos(\tilde{\kappa}_B L)\cosh(\tilde{\kappa}_B L)+1]}, \tag{87}$$

$$\frac{\partial^2\xi(x)}{\partial x^2} = \frac{f_0[A\exp(\mathrm{j}\tilde{\kappa}_B x) + B\exp(-\mathrm{j}\tilde{\kappa}_B x) - C\exp(\tilde{\kappa}_B x) - D\exp(-\tilde{\kappa}_B x)]}{2\tilde{\mathrm{E}}I\tilde{\kappa}_B[\cos(\tilde{\kappa}_B L)\cosh(\tilde{\kappa}_B L)+1]}. \tag{88}$$

The squared-magnitude of $\partial^2\xi(x)/\partial x^2$ is expressed as

$$\left|\frac{\partial^2\xi(x)}{\partial x^2}\right|^2 = \frac{\partial^2\xi(x)}{\partial x^2}\cdot\left[\frac{\partial^2\xi(x)}{\partial x^2}\right]^* = Q_4\left[\frac{\left|f_0\right|^2}{4\left|\tilde{\mathrm{E}}\right|^2 I^2|\tilde{\kappa}_B|^2\left|\cos(\tilde{\kappa}_B L)\cosh(\tilde{\kappa}_B L)+1\right|^2}\right], \tag{89}$$

$$Q_4 = \begin{bmatrix} |A|^2\exp(-2\kappa''_B x) + |B|^2\exp(2\kappa''_B x) + |C|^2\exp(2\kappa'_B x) + |D|^2\exp(-2\kappa'_B x) \\ +2\cdot\mathrm{Re}\begin{bmatrix} AB^*\exp(2\mathrm{j}\kappa'_B x) + CD^*\exp(2\mathrm{j}\kappa''_B x) \\ -AC^*\exp[(\kappa'_B-\kappa''_B)(1+\mathrm{j})x] - AD^*\exp[(\kappa'_B+\kappa''_B)(-1+\mathrm{j})x] \\ -BC^*\exp[(\kappa'_B+\kappa''_B)(1-\mathrm{j})x] - BD^*\exp[(-\kappa'_B+\kappa''_B)(1+\mathrm{j})x] \end{bmatrix} \end{bmatrix}. \tag{90}$$

Similarly, time-averaged potential and dissipated energies are derived as follows by integrating $\left|\partial^2\xi(x)/\partial x^2\right|$ over the beam span:

$$\bar{E}_k(\omega) = \frac{\mathrm{E}'I}{2}\int_0^\infty \left|\frac{\partial^2\xi(x)}{\partial x^2}\right|^2 \mathrm{d}x = [Q_2 + Q_5]\left[\frac{\mathrm{E}'\left|f_0\right|^2}{8\left|\tilde{\mathrm{E}}\right|^2 I|\tilde{\kappa}_B|^2\left|\cos(\tilde{\kappa}_B L)\cosh(\tilde{\kappa}_B L)+1\right|^2}\right], \tag{91}$$

$$\bar{E}_d(\omega) = \frac{\mathrm{E}''I}{2}\int_0^\infty \left|\frac{\partial^2\xi(x)}{\partial x^2}\right|^2 \mathrm{d}x = [Q_2 + Q_5]\left[\frac{\mathrm{E}''\left|f_0\right|^2}{8\left|\tilde{\mathrm{E}}\right|^2 I|\tilde{\kappa}_B|^2\left|\cos(\tilde{\kappa}_B L)\cosh(\tilde{\kappa}_B L)+1\right|^2}\right], \tag{92}$$

$$Q_5 = 2 \cdot \mathrm{Re}\begin{bmatrix} AB^*\left[\exp(2\mathrm{j}\kappa'_B L) - 1\right]/(2\mathrm{j}\kappa'_B) + CD^*\left[\exp(2\mathrm{j}\kappa''_B L) - 1\right]/(2\mathrm{j}\kappa''_B) \\ -AC^*\left[\exp((\kappa'_B - \kappa''_B)(1+\mathrm{j})L) - 1\right]/((\kappa'_B - \kappa''_B)(1+\mathrm{j})) \\ -AD^*\left[\exp((\kappa'_B + \kappa''_B)(-1+\mathrm{j})L) - 1\right]/((\kappa'_B + \kappa''_B)(-1+\mathrm{j})) \\ -BC^*\left[\exp((\kappa'_B + \kappa''_B)(1-\mathrm{j})L) - 1\right]/((\kappa'_B + \kappa''_B)(1-\mathrm{j})) \\ -BD^*\left[\exp((-\kappa'_B + \kappa''_B)(1+\mathrm{j})L) - 1\right]/((-\kappa'_B + \kappa''_B)(1+\mathrm{j})) \end{bmatrix}. \quad (93)$$

Like the longitudinal motion, the same result for $\bar{E}_d$ can also be obtained by using Eq. (66).

7. Role of damping

Now, the time-averaged energies are calculated and the energy input measures are compared via the ratios (Δ) of two alternate systems with high ($\eta_2 = 0.2$) and low ($\eta_2 = 0.08$) loss factors. Three spectrally-varying insertion losses of time-averaged kinetic, potential and dissipated energies are defined here as

$$\Delta(\bar{E}_m;\omega) = \frac{\bar{E}_m \text{ with } \eta_2}{\bar{E}_m \text{ with } \eta_1}, \quad \Delta(\bar{E}_k;\omega) = \frac{\bar{E}_k \text{ with } \eta_2}{\bar{E}_k \text{ with } \eta_1}, \quad \Delta(\bar{E}_d;\omega) = \frac{\bar{E}_d \text{ with } \eta_2}{\bar{E}_d \text{ with } \eta_1}. \quad (94-96)$$

Results are shown in Fig. 7 where the same forces are applied to the system of Fig. 6 with η_1 and η_2. Fig. 7 shows that $\Delta(\bar{E}_m)$ approaches η_2/η_1 ratio at higher frequencies. However, it is observed that $\Delta(\bar{E}_d)$ converges to unity. Essentially, $\bar{E}_d$ makes no distinction between two systems at higher frequencies, unlike $\bar{E}_m$. This implies that the $\bar{E}_d$ ratio with higher and lower damping systems respectively remain the same at higher frequencies due to the following reasons: (1) $\bar{E}_d$ can be approximately represented as $\bar{E}_d \approx \eta \cdot \bar{E}_k \approx \eta \cdot \bar{E}_m$ at high frequencies; (2) $\bar{E}_m$ with a highly damped system is lower than the one with a lightly damped system as expected; (3) $\bar{E}_d$ with higher η and lower $\bar{E}_m$ becomes equal to the one with lower η and higher $\bar{E}_m$. Hence, the dissipated

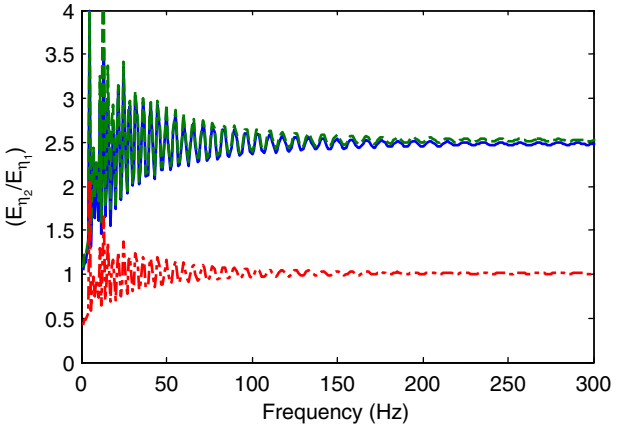

Fig. 7. Ratios of time-averaged energy for flexural motions of a clamped-free beam of Fig. 6(b) given a force excitation at the free end. Here, $\eta_2 = 0.2$ and $\eta_1 = 0.08$. Key: ——, $\Delta(\bar{E}_m)$; ——, $\Delta(\bar{E}_k)$, ——, $\Delta(\bar{E}_d)$.

energy may not exhibit much reduction by the application of high damping although the kinetic energy input is significantly diminished at higher frequencies. Consequently, caution must be exercised when choosing a vibrational energy input as a vibration transmission measure. Conversely, Fig. 7 shows that $\Delta(\bar{E}_m)$ is unity and $\Delta(\bar{E}_d)$ displays the η_1/η_2 relationship (inverse of the ratio of loss factors) at very low frequencies. This indicates that the introduction of high damping would increase $\bar{E}_d$ but $\bar{E}_m$ would remain the same at lower frequencies. Further, $\Delta(\bar{E}_m)$ and $\Delta(\bar{E}_k)$ are found to be very close each other at all frequencies. Finally, the $\Delta(\bar{E}_k)/\Delta(\bar{E}_d)$ ratio expression is give by η_2/η_1, as expected.

8. Comparison of Methods 2 and 3

Next, two energy characterization methods are again compared. The estimates for the sum of time-averaged kinetic and potential energies from Method 3 are calculated for longitudinal motions of Fig. 6(a) and are compared with the ones from Method 2 in Fig. 8. Like the discrete system, both Methods 2 and 3 come very close to the exact kinetic and potential energies but the deviations increase as damping and frequency increase. Further, Method 3 produces most consistent predictions using both impedance and mobility formulations while Method 2 exhibits results that are formulation sensitive. Furthermore, many spurious peaks are observed in Fig. 8 for the estimates from Method 2, like the discrete system case. Fig. 8(a), (c) also shows that $\bar{E}_m + \bar{E}_k$ from Method 2 with impedance deviates more from around 450 Hz and yields negative values at the end of frequency band. This magnified deviation results from the odd number of zero crossing points within the frequency band that Method 2 utilizes. Recall from the earlier discussion, the numerical modeling and compensation procedure of Method 2 requires a pair of the zero crossing points.

Calculated results for the flexural motions of the clamped–free beam of Fig. 6(b) are shown in Fig. 9. Similar to the longitudinal motion case, both $\hat{\bar{E}}_{2m} + \hat{\bar{E}}_{2k}$ and $\hat{\bar{E}}_{3m} + \hat{\bar{E}}_{3k}$ estimate are close to the exact values but the deviations between the estimates and the exact ones are again observed as the frequency and damping increase. Like the previous case, Fig. 9 shows that $\hat{\bar{E}}_{3m} + \hat{\bar{E}}_{3k}$ produces erroneous peaks and the mobility and impedance formulations yield different results. Conversely, Method 3 estimates the same results from impedance and mobility, like the previous example for longitudinal motions.

9. Conclusion

Three energy characterization methods have been critically examined in this article for discrete and continuous systems over the low and mid frequency regimes. Methods 1 and 2, as proposed by Bobrovnitskii and Korotkov [8,9], yield inconsistent estimates when mobility and/or impedance formulations are compared. Their estimates deviate from the actual energy inputs as the frequency and/or damping increases. Further, Method 2 requires additional knowledge of the transfer functions and yet its energy estimate is sensitive to the numerical correction factors. To overcome the deficiencies of Methods 1 and 2, we have proposed a new formulation (Methods 3) for the spectral energy characterization that is based on a correct

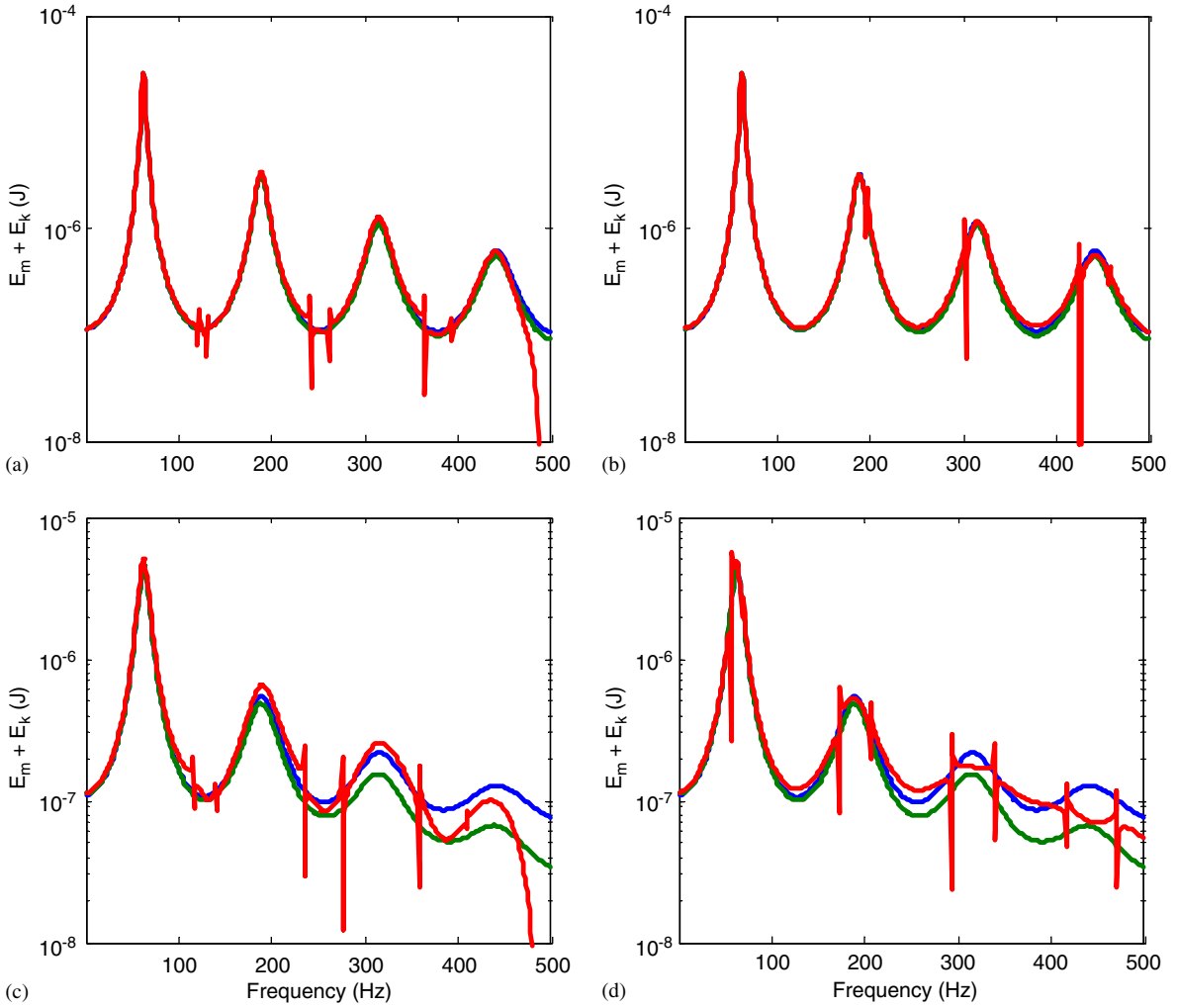

Fig. 8. Sum of time-averaged kinetic and potential energies for longitudinal motions of a clamped-free beam of Fig. 6(a) given a force excitation at the free end:(a) lightly damped system ($\eta = 0.08$) with impedance; (b) lightly damped system ($\eta = 0.08$) with mobility; (c) heavily damped system ($\eta = 0.2$) with impedance; (d) heavily damped system ($\eta = 0.2$) with mobility. Key: ———, Exact; ———, Method 3, ———, Method 2.

interpretation of the driving point mobilities or impedances. Method 3 is insensitive to the driving point mobility or impedance formulations and yields consistent results, unlike the existing methods (1 and 2). Further, our method does not require any prior knowledge of the transfer functions, unlike Method 2. Nonetheless, Method 3 still shows some discrepancies near resonances as the structural damping is increased. Therefore, further work is required to improve our methodology especially over the high frequency regime and to develop the energy characterization schemes when multiple phase-correlated sinusoidal force excitations are applied to a vibratory system.

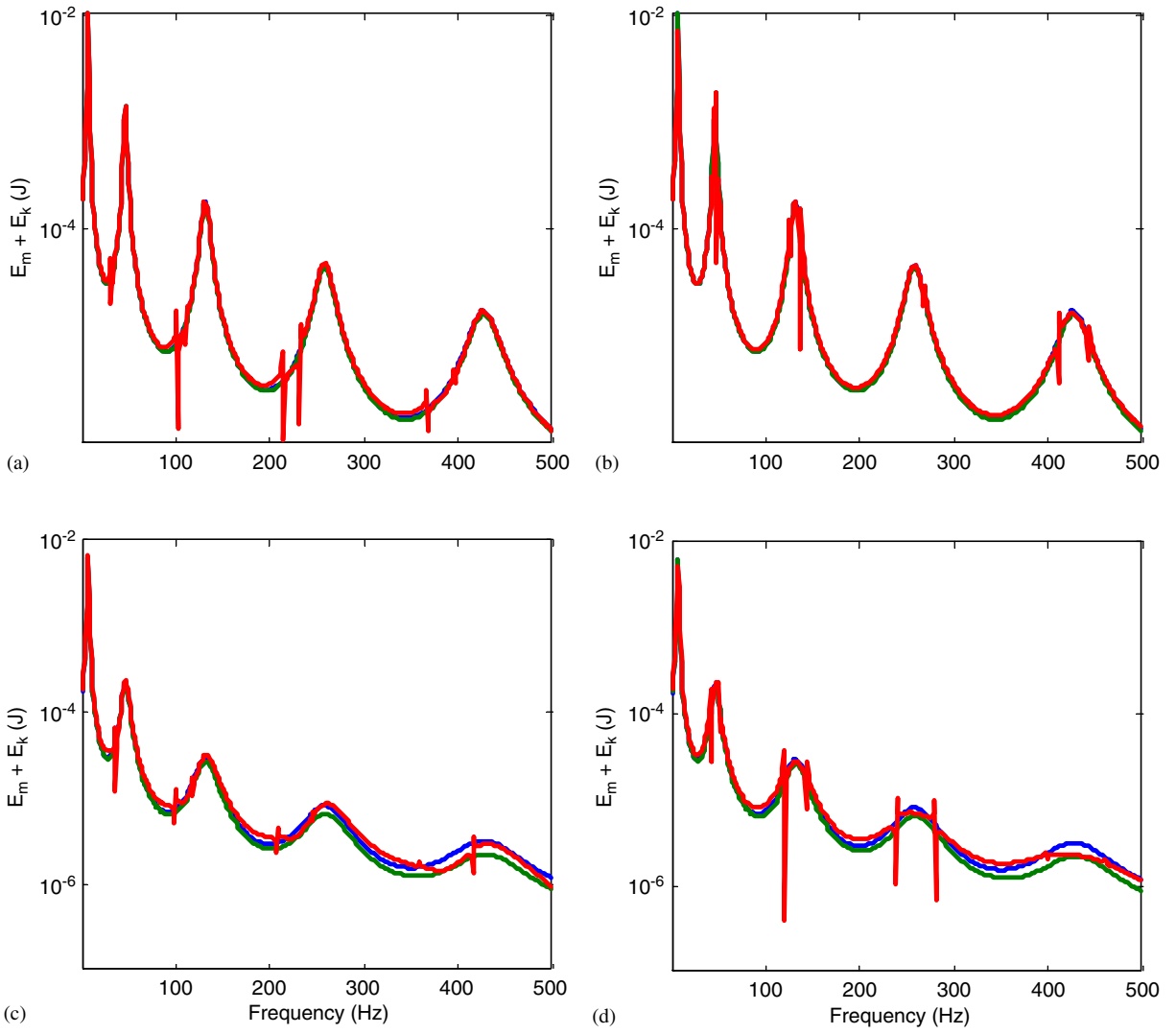

Fig. 9. Sum of time-averaged kinetic and potential energies for flexural motions of a clamped–free beam of Fig. 6(b) given a force excitation at the free end: (a) lightly damped system ($\eta = 0.08$) with impedance; (b) lightly damped system ($\eta = 0.08$) with mobility; (c) heavily damped system ($\eta = 0.2$) with impedance; (d) heavily damped system ($\eta = 0.2$) with mobility. Key: ——, Exact; ——, Method 3, ——, Method 2.

Acknowledgment

The Center for Automotive Research Industrial Consortium at The Ohio State University is gratefully acknowledged for supporting this research.

References

[1] L. Cremer, M. Heckle, *Structure-Borne Sound: Structural Vibrations and Sound Radiation at Audio Frequencies*, Springer, New York, 1973.
[2] J.L. Wohlever, R.J. Bernhard, Mechanical energy flow models of rods and beams, *Journal of Sound and Vibration* 153 (1) (1992) 1–19.
[3] R. Singh, S. Kim, Examination of multi-dimensional vibration isolation measures and their correlation to sound radiation over a broad frequency range, *Journal of Sound and Vibration* 262 (3) (2003) 419–455.
[4] S. Kim, R. Singh, Vibration transmission through an isolator modeled by continuous system theory, *Journal of Sound and Vibration* 248 (5) (2001) 925–953.
[5] T.E. Rook, R. Singh, Mobility analysis of structure-borne noise power flow through bearings in gearbox-like structures, *Noise Control Engineering Journal* 44 (2) (1996) 69–78.
[6] R.H. Lyon, R.G. Dejong, *Theory and Application of Statistical Energy Analysis*, Butterworth-Heinemann, Boston, 1995.
[7] G. Pavic, The role of damping on energy and power in vibrating systems, *Journal of Sound and Vibration* 281 (2005) 45–71.
[8] Y.I. Bobrovnitskii, Estimating the vibrational energy characteristics of an elastic structure via the input impedance and mobility, *Journal of Sound and Vibration* 217 (2) (1998) 351–386.
[9] Y.I. Bobrovnitskii, M.P. Korotkov, Improved estimates for the energy characteristics of a vibrating elastic structure via the input impedance and mobility: experimental verification, *Journal of Sound and Vibration* 247 (4) (2001) 683–702.